Colloidal particles interacting with a polymer brush: a self-consistent field theory

Mikhail Laktionov, Oleg Shavykin, Frans Leermakers, Ekaterina Zhulina, Oleg Borisov

Colloidal particle interacting with a polymer brush: a self-consistent field theory.

Mikhail Y.Laktionov[1], Oleg V.Shavykin[1], Frans A.M.Leermakers[2], Ekaterina B.Zhulina[1,3],Oleg V. Borisov[1,3,4],
[1]St.Petersburg National Research University of Information Technologies, Mechanics and Optics, 197101 St.Petersburg, Russia
[2]Physical Chemistry and Soft Matter, Wageningen University, 6703 NB Wageningen, The Netherlands,
[3]Institute of Macromolecular Compounds of the Russian Academy of Sciences, 199004 St.Petersburg, Russia
[4] CNRS, Université de Pau et des Pays de l'Adour UMR 5254, Institut des Sciences Analytiques et de Physico-Chimie pour l'Environnement et les Matériaux, Pau, France

February 13, 2022

email: oleg.borisov@uiv-pau.fr

Abstract

Interaction of colloidal particle with planar polymer brush immersed into a solvent of variable thermodynamic quality is studied by numerical self-consistent field method combined with analytical mean-field theory. The effect of embedded particle on the distribution of polymer density in the brush is analyzed and the particle insertion free energy profiles are calculated for variable size and shape of the particle and sets of polymer-particle and polymer-solvent interaction parameters. In particular, both cases of repulsive and attractive interactions between particle and brush-forming chains are considered. It is demonstrated that for large particles the insertion free energy is dominated by repulsive (osmotic) contribution and is approximately proportional to the particle volume in accordance with earlier theoretical predictions [Halperin, A. et al, Macromolecules 2011, 44,3622].

For the particles of smaller size or/and large shape asymmetry the adsorption or depletion of polymer from the particle surface essentially contributes to the insertion free energy balance. As a result, depending on the set of the polymer-solvent and polymer-particle interaction parameters and brush grafting density the insertion free energy profile may exhibit complex patterns, i.e., from pure repulsive effective potential barrier to attractive well. The results of our study allow for predicting equilibrium partitioning and controlling diffusive transport of (bio)nanocolloids across (bio)polymer brushes of arbitrary geometry including polymer-modified membranes or nanopores.

1 Introduction

Understanding transport and partitioning of nanocolloids and large molecules in polymeric media, e.g., concentrated solutions, melts, gels, promotes comprehension of processes occurring in technological applications (separation, purification) and living tissues. The principals of selective transport and partitioning of macromolecules adopted from nature can be successfully exploited in bioinspired nanotechnology.

For instance, the membranes of bacterial and endothelial cells are decorated by anchored biopolymers (lipopolysaccharides, glycoproteins) that form brushlike interfacial layers.[1–4] Similar structural motif for intrinsically disordered proteins is found inside nucleopores perforating membrane of nucleus. These brushlike arrays of biopolymers constitute steric penetration barriers providing selective permeability of globular proteins and macromolecules.[5–10]

In the realm of medicine, polymer brushes formed by biocompatible hydrophilic polymers, e.g. PEG, PMOXA etc. are used for fabrication of biocompatible non-fouling surfaces[11–17] of artificial implants and medical devices, as well as providing stealth properties for nanoscale drug delivery systems.[18–22] In spite of broad use, the mechanisms of interaction (selective penetration, accumulation or expulsion) of (bio)nanocolloidal particles, first of all globular proteins, in polymer brushes are still not fully understood.

In particular, balance of steric repulsive and short-range attractive interactions between brush-forming polymers and particles may have an impact on dependencies of the partition coefficients on the size of the particles and brush grafting density. There are indications from experiments that some proteins, e.g. BSA, may exhibit weak affinity to PEG chains and therefore accumulate in PEG brushes.[23,24] Furthermore, solubility of partially hydrophobic or thermosensitive brush-forming chains may provide additional control parameters for manipulating partitioning and transport of bionanocolloids through polymer brushes.

Theories of interactions of nanocolloids with planar polymer brushes were developed in the past decades mostly on the basis of strong stretching self-consistent field approximation. In solvent-free (dry) brushes, a penalty for nanoparticle insertion was described in terms of the pressure field acting at nano-object.[25] Polymer-soluble nanoparticles smaller than a brush-determined threshold were shown to disperse in the film to a depth scaling inversely with particle volume. In solvated brushes penetration of nano-objects, e.g., small proteins[26,27] and ultrathin AFM tips[28] invoked short ranged perturbation of the brush concentration profile, in agreement with the simulation results.[29,30]

In the seminal paper by Halperin et al[31] a fundamental relation between

particle insertion free energy and osmotic pressure inside a planar polymer brush was established. This theory accounted for the thermodynamic quality of the solvent to quantify the osmotic contribution to the insertion free energy of nano-object. The latter was proportional to the particle volume, depended on the particle-solvent interactions, and served as a good approximation for sufficiently large particles. However, for particles of smaller size (comparable to polymer density correlation length) such approximation becomes inaccurate. Furthermore, the details of short-range interactions between monomer units of the brush-forming chains and particle surface are crucially important and may strongly affect the shape of the insertion free energy profiles and thus particle transport through the brush.

The aim of the present paper is to study interaction of nanocolloidal particle with non-ionic polymer brush and calculate the position-dependent insertion free energy with the account of most relevant interactions, particle size and shape and brush grafting density. The effect of embedded particle on the density distribution of polymer in the brush was analyzed as well. Knowledge of the shape of the free energy versus particle position curves does not only allow predicting equilibrium distribution of particles between the brush and solution, but also paths the way to study diffusion of particles across polymer-modified membranes. Because of the high complexity of the system, the problem cannot be adequately treated neither analytically, nor with the aid of direct computer simulations, which would require long computational times for exploring relevant range of control (thermodynamic solvent quality for polymers, polymer-particle interaction) and architectural (polymer grafting density, particle size and shape) parameters. Therefore, we employ molecular realistic self-consistent field modelling which is the most appropriate technique. Specifically, we use the Scheutjens-Fleer self-consistent field (SF-SCF) lattice method[32] in its two-gradient version. The SF-SCF numerical method allows obtaining structural and thermodynamic properties of complex polymer systems with the accuracy close to that provided by coarse-grained molecular simulation (Brownian Dynamics, Monte Carlo) techniques, but with orders of magnitude higher computational efficiency, that is crucial in sdudies of many-chains systems (e.g. polymer brushes). On the other hand, this method is free of many approximations (e.g., strong stretching of polymer chains) unavoidably used by analytical theory of polymer brushes. The comparison of the obtained numerical results to those derived within simplified analytical model enables us to rationalize the main features in the insertion free energy patterns and, at the same time, to estimate accuracy and identify limits of applicability of the mean-field analytical approach.

The rest of the paper is organized as follows:

We start in Section 2 with brief reviewing principles of analytical the-

ory of polymer brushes in solvent of arbitrary quality based on analytical strong-stretching self consistent field (SS-SCF) approximation and formulate analytical approach for calculating insertion free energy of a particle into the brush in Section 3. In Section 4 we present results of our numerical calculations for variable polymer-particle interaction parameter and solvent quality for the brush-forming chains and confront them to the results derived using analytical theory. Finally, in Section 5 we summarize our conclusions.

2 Analytical theory of polymer brushes: polymer concentration profile and osmotic pressure

We consider a brush formed by long flexible polymer chains with degree of polymerization (DP) N and one unit length Kuhn segment grafted by one end to an impermeable planar surface and immersed into a solvent. The grafting density is characterized by the area per chain s (or the inverse value σ). The solvent quality is characterized by the Flory-Huggins parameter χ_{PS} where subscript PS refers to polymer-solvent interactions.

Theory of structural properties of planar polymer brushes formed by non-ionic polymer chains in solvent of arbitrary thermodynamic quality was developed in original papers of the authors[33–35] where a virial approximation valid at small volume fraction of monomer units in the brush, $\phi \ll 1$, was employed. The virial approximation accounts only for binary and ternary monomer-monomer interactions in the brush and allows for exploring properties of relatively sparsely grafted brushes under good or close to theta-solvent conditions. Below we formulate a more general scheme which is operative at arbitrary polymer concentration. This allows us to explore the effects of solvent strength and polymer-particle interactions in a wide range of parameters, including collapsed in poor solvent brushes with polymer volume fraction approaching unity, $\phi \simeq 1$.

Within the analytical strong-stretching self-consistent field (SS-SCF) approximation the self-consistent molecular potential inside the brush exhibits a parabolic dependence on the distance z from the grafting surface.

$$\frac{\partial f\{\phi(z)\}}{\partial \phi(z)} = \frac{3}{2}\kappa^2(\Lambda^2 - z^2) \tag{1}$$

where $\phi(z)$ is the profile of volume fraction of monomer units in the brush, $f\{\phi(z)\}$ is the free energy of interactions in the brush per unit volume, κ is

a coefficient dependent on the DP and topology of the brush-forming chains (for linear chains $\kappa = \pi/2N$) and parameter Λ is specified below.

Eq. 1 presumes Gaussian (linear) conformational elasticity of the brush-forming chains on all the length scales and absence of dead zones proximal to the grafting surface and depleted of the chain ends. Remarkably eq 1 is applicable irrespectively of the specific type of interactions (functional form of $f\{\phi(z)\}$) in the brush. Here we apply the mean field Flory-Huggins approximation

$$\frac{f\{\phi(z)\}}{k_BT} = (1-\phi(z))\ln(1-\phi(z)) + \chi_{PS}\phi(z)(1-\phi(z)) + \phi(z)(1-\chi_{PS}) \quad (2)$$

Combining eqs 1 and 2 we obtain implicit dependence of the polymer volume fraction in the brush on z as

$$-\ln(1-\phi(z)) - 2\chi_{PS}\phi(z) = \frac{3}{2}\kappa^2(\Lambda^2 - z^2) \quad (3)$$

The cut-off length for polymer volume fraction profile (the brush thickness) D has to be found from the normalization condition

$$\int_0^D \phi(z)dz = \frac{N}{s} \quad (4)$$

The osmotic pressure inside the brush is given by

$$\Pi(z) = \phi(z)\frac{\partial f\{\phi(z)\}}{\partial\phi(z)} - f\{\phi(z)\} =$$
$$k_BT[-\ln(1-\phi(z)) - \phi(z) - \chi_{PS}\phi^2(z)] \approx$$
$$k_BT[(\frac{1}{2} - \chi_{PS})\phi^2(z) + \frac{1}{3}\phi^3(z) + ...] \quad (5)$$

where the last equality corresponds to the virial expansion in terms of ϕ valid at $\phi \ll 1$.

If we define the polymer volume fraction at the edge of the brush, $z = D$ as $\phi(D) \equiv \phi_D$, then, from the condition of vanishing osmotic pressure at the edge of the brush, $\Pi(z = D) = 0$, we find an equation for ϕ_D as a function of χ_{PS}

$$-\ln(1-\phi_D) - \phi_D - \chi_{PS}\phi_D^2 = 0 \quad (6)$$

By substituting $z = D$ into eq 3 we find that

$$\Lambda^2 = D^2 - \frac{2}{3\kappa^2}[\ln(1-\phi_D) + 2\chi_{PS}\phi_D] \quad (7)$$

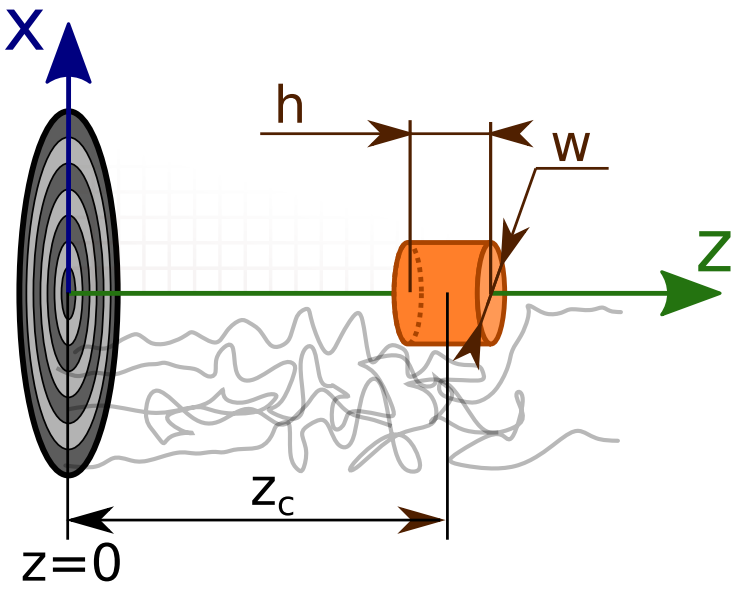

Figure 1: Cylindrical colloidal particle embedded in a polymer brush, schematic representation of SF-SCF 2-gradient version implementation with cylindrical symmetry. Concentric circles on the left side represents grafting surface ($z = 0$), the particle center position is denoted as z_c, particle diameter and height are w and h, respectively.

As follows from eq 6, $\phi_D = 0$ at $\chi_{PS} \leq 1/2$, (i.e., under good or theta-solvent conditions) and $\phi_D \geq 0$ at $\chi_{PS} \geq 1/2$ (poor solvent conditions). Evidently, under poor solvent conditions ϕ_D defined by eq 6 coincides with the polymer volume fraction in a large globule (precipitate polymer phase). Then, as follows from eq 7, $\Lambda^2 = D^2$ at $\chi_{PS} \leq 1/2$ and $\Lambda^2 \leq D^2$ at $\chi_{PS} \leq 1/2$.

3 Free energy of the particle insertion into the brush: an analytical approach

Without major loss of generality and having in mind implementation of SF-SCF numerical self-consistent field scheme in its 2-gradient version, we consider the brush with embedded particle which possesses cylindrical symmetry with respect to the axis perpendicular to the grafting surface (Figure 1).

Let the z-coordinate of the center of the particle be z_c. The radius of the particle is described by the function $r_c(z')$, where $z' \in [z_c - h/2, z_c + h/2]$ and h is the dimension of the particle in the z direction.

If one can neglect gradient in polymer density inside the brush in the z-direction on the length scale of the order of the particle size, $h \cdot |d\phi(z)/dz| \ll$

$\phi(z)$, then the insertion free energy (with the reference state of the particle outside the brush) can be approximated as

$$\begin{aligned}\Delta F(z_c) =&\Delta F_{osm}(z_c) + \Delta F_{surf}(z_c) = \\ &\Pi(z_c) \cdot V + \gamma\{\phi(z_c)\} \cdot A\end{aligned} \tag{8}$$

where

$$V = \pi \int_{z_c-h/2}^{z_c+h/2} r_c^2(z')dz' \tag{9}$$

and

$$\begin{aligned}A = 2\pi \int_{z_c-h/2}^{z_c+h/2} [r_c(z')+&\frac{1}{2}\delta(z' - (z_c - h/2))r_c^2(z')+ \\ &\frac{1}{2}\delta(z' - (z_c + h/2))r_c^2(z')]dz'\end{aligned} \tag{10}$$

are the volume and the surface area of the particle, respectively and $\gamma\{\phi(z_c)\}$ is the excess free energy per unit area of the particle in contact with polymer solution of concentration $\phi(z_c)$.

A more general expression for the insertion free energy which we use in our numerical calculations is

$$\begin{aligned}\Delta F(z_c) = \pi \int_{z_c-h/2}^{z_c+h/2} \Pi(z')r_c^2(z')dz'+ \\ 2\pi \int_{z_c-h/2}^{z_c+h/2} \gamma\{\phi(z')\}[r_c(z') + \frac{1}{2}\delta(z' - (z_c - h/2))r_c^2(z')+ \\ \frac{1}{2}\delta(z' - (z_c + h))r_c^2(z')]dz'\end{aligned} \tag{11}$$

Eqs 8, 11 without the second (proportional to the particle surface) term are equivalent to those derived in ref.[31] Importantly, the particle is treated as a probe, that is, upon evaluating ΔF we use unperturbed profiles of polymer concentration $\phi(z)$ and osmotic pressure $\Pi(z)$ in the brush (in the absence of a particle). Moreover, splitting of the insertion free energy into volume and surface terms is justified only if the particle size is much larger than the width of the zone of perturbed by the particle polymer density distribution (the correlation length or adsorbtion layer thickness). As demonstrated below, a significant deviation between approximate analytical and exact numerical results are found for small particles.

The insertion free energy $\Delta F(z_c)$ is directly related to the partition coefficient $K(z_c) = \exp(-\Delta F(z_c)/k_BT)$. The particles can be either expelled

from the brush, $K \leq 1$ (depletion regime) or accumulated in the brush, $K \geq 1$ (absorption regime). The concentration of particles inside the brush is either small or larger than in the bulk of the solution at $K \leq 1$ or $K \geq 1$, respectively.

While the volume contribution to the insertion free energy (the first term in eq. 8 or 11) is always positive, since $\Pi(\phi(z)) \geq 0$, the sign of particle surface contribution (the second term in eq 8 or 11 proportional to γ) depends on polymer-particle interactions and can be either positive or negative depending on the set of interaction parameters, $\{\chi_{PS}, \chi_{PC}, \chi_{CS}\}$, and local concentration of polymer $\phi(z)$, i.e $\gamma(z) = \gamma\{\chi_{PS}, \chi_{PC}, \chi_{CS}; \phi(z)\}$. Here $\chi_{PS}, \chi_{PC}, \chi_{CS}$ describe direct polymer-solvent (PS), polymer-colloid (PC) and colloid-solvent (CS) interactions, respectively, within employed below discrete lattice model. Without loss of generality we set $\chi_{CS} = 0$. Then physically relevant control parameter describing polymer-colloid interaction is

$$\chi_{ads} = \chi_{PC} - \chi_{PS}(1 - \phi) \tag{12}$$

(free energy change upon replacement of a contact of monomer unit with solvent by a contact with the surface).

If the surface of the particle is repulsive ($\chi_{ads} \geq 0$) or even weakly attractive ($\chi_{ads}^{(crit)} \leq \chi_{ads} < 0$) for polymers, then, because of imposed by the impermeable surface steric constraint on the available set of polymer conformations, polymer is depleted from the particle surface and $\gamma \geq 0$. At $\chi_{ads} = \chi_{ads}^{(crit)}$ conformational entropy losses due to presence of the surface and free energy gain upon monomer-surface contact cancel each other and γ vanishes.[32,36–38] The value of $\chi_{ads}^{(crit)}$ depends on the local properties of the lattice where polymer chain performs its random walk. For the simple cubic lattice $\chi_{ads}^{(crit)} = 6ln(5/6)$. Finally, at $\chi_{ads} \leq \chi_{ads}^{(crit)}$ polymer is sufficiently strongly attracted to the surface of the particle and forms enriched by polymer adsorbed layer entrapping the particle, and $\gamma \leq 0$.

The difference $\chi_{ads} - \chi_{ads}^{(crit)}$ serves as a universal parameter characterizing switch between adsorption and depletion regimes at vanishing polymer concentration. However, as it will be confirmed below by SF-SCF calculations, $\gamma(z)$ varies throughout the brush and exhibits more complex dependence on $\phi(z)$ than it follows from eq 12. Furthermore, for small particles $\chi_{ads}^{(crit)}$ and γ may exhibit dependence on the surface curvature.

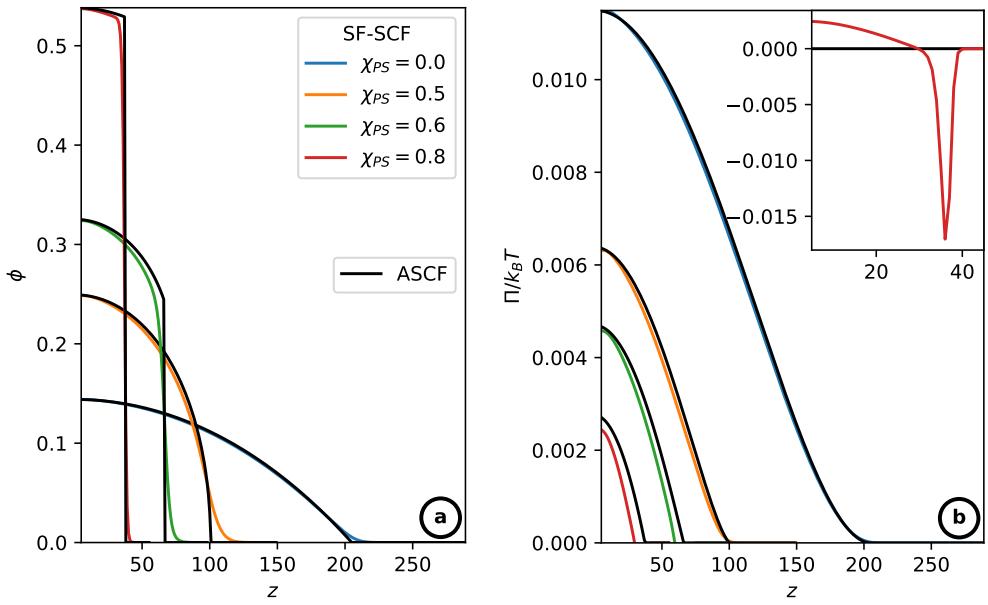

Figure 2: Polymer density (a) and osmotic pressure profile (b).
Strong stretching self-consistent approximation (ASCF) and SF-SCF numerical results at $\chi_{PS} = \{0, 0.5, 0.6, 0.8\}$ for $N = 1000$, $\sigma = 0.02$

4 Particle insertion into the brush: the SF-SCF numerical results

4.1 Impact of an embedded particle on the brush structure

For numerical SF-SCF calculations of the particle insertion a polymer brush with a degree of polymerization $N = 1000$ and the grafting density of $\sigma = 0.02$ has been selected. The embedded particle has a cylindrical shape, with the height h and the diameter of the base w. The symmetry axis of the cylindrical particle is directed perpendicular to the grafting surface and coincides with the z-axis of our cylindrical coordinate system. (Figure 1).

As shown in Figures 2a and 2b the profiles of polymer density $\phi(z)$ and the profiles of osmotic pressure $\Pi(z)$ calculated analytically (SS-SCF) and numerically (SF-SCF) for particle-free brush at different values of χ_{PS} ranging from good ($\chi_{PS} = 0$) to theta- ($\chi_{PS} = 1/2$) and poor ($\chi_{PS} \geq 1/2$) solvents almost perfectly match each other. A smoother decay in the numerically calculated density profiles near the edge of the brush are due to non-stretched terminal segments of the chains that exhibit Gaussian fluctu-

ations not accounted for in the SS-SCF scheme. For plotting "numerical" osmotic pressure profiles $\Pi(z)$ presented in Figure 2b we used analytical eq 5 where numerically calculated by SF-SCF density profiles $\phi(z)$ were substituted. A contraction of the brush caused by decreasing solvent strength is accompanied by an increase in polymer density inside the brush and concomitant decrease in the osmotic pressure. A zone of negative osmotic pressure appearing under poor solvent conditions ($\chi_{PS} \geq 1/2$) close to the edge of the brush is a manifestation of positive surface tension at the interface between collapsed polymer brush and poor solvent.[39]

Two-gradient SF-SCF calculations of a polymer brush with an embedded particle allows obtaining detailed information about spatial polymer density distribution in the brush. In Figures 3, 4 spatial polymer density diagrams and profiles are presented for the brush with an embedded particle.

An embedded particle causes perturbation of the polymer density distribution both in the directions perpendicular ($z-axis$) and parallel ($x-axis$) to the grafting surface, as one can see it as a halo of different color around the particle in Figures 3 or wells in Figure 4.

Let us take a closer look on the polymer density depletion and enrichment regions. To examine disturbances in polymer density a volume (highlighted with a red borders rectangle in upper right frame of Figure 3a) proximal to an embedded particle replotted in Figure 3b in a different scale. The sequence which diagrams are presented in corresponds to the ones on Figure 3a and follows the next order $\chi_{PC} = [[-0.5, -0.75][-1.0, -1.25]]$.

The diagrams of Figure 4 show the difference between an unperturbed particle-free polymer brush and a polymer brush with an embedded particle $\phi - \phi^*$, where ϕ^* is the polymer concentration of the corresponding unperturbed polymer brush. The difference $\phi - \phi^*$ is color-coded with diverging color scale, where blue color means polymer depletion, red color means an excess of polymer, while white means that the polymer concentration remains unchanged.

In Figure 4 the polymer concentration profiles in z- (Figure 4a, 4b) and in x- directions (Figure 4c) are plotted. (The x-axis perpendicular to the z-axis z has its origin in the particle center z_c). Figure 4a illustrates polymer concentration of an unperturbed brush $\phi^*(z)$ and the ones with an embedded particle of the same size and position but different affinity to the polymer ($\chi_{PC} = \{-0.5, -0.75, -1.0, -1.25\}$). To make the profiles in the vicinity of the particle easier to trace we present Figure 4b as a zoomed version.

Note that the polymer concentration profiles in the lateral x-direction in unperturbed brush (Figure 4c) has the shape of a straight horizontal line, meaning no disturbances in the brush when no particle is introduced.

In the case of weakly attractive particle $\chi_{PC} = -0.5$ (the upper left

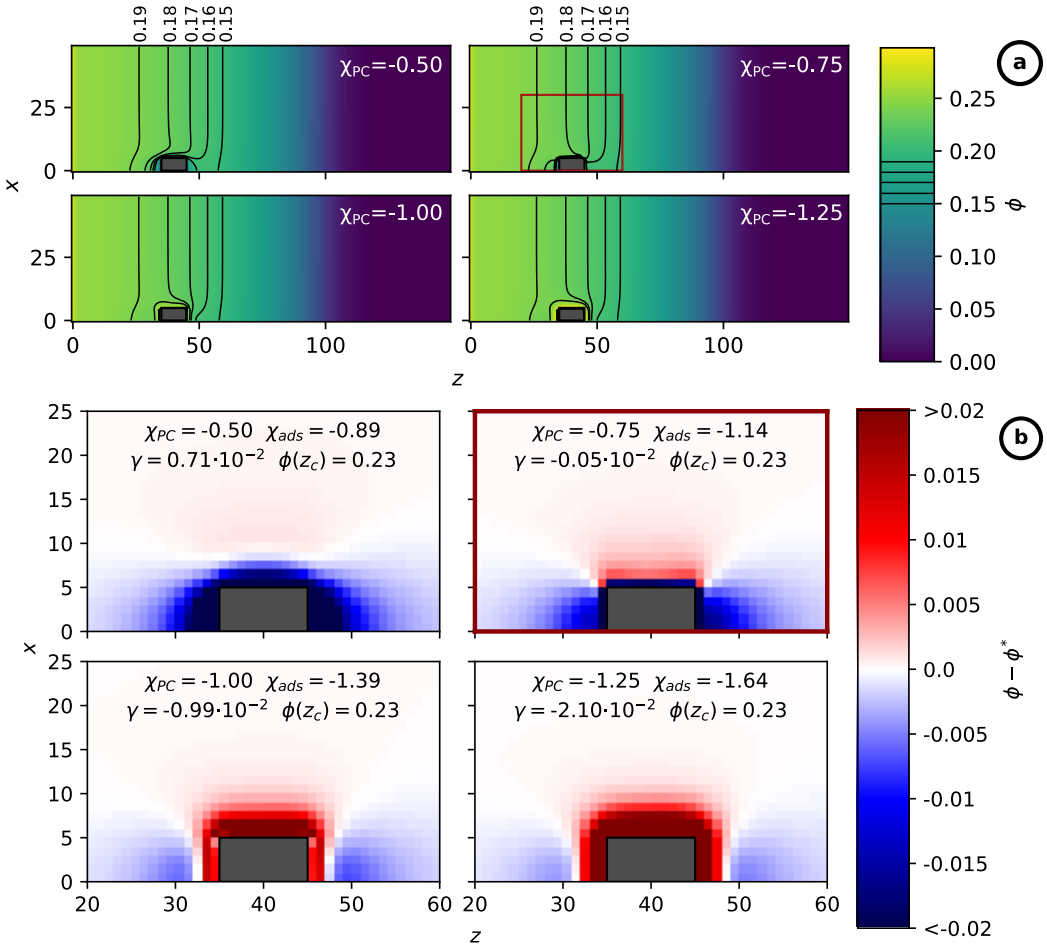

Figure 3: Perturbation of the polymer density in a brush caused by an embedded particle for $z_c = 40$, $h = w = 10$, $\chi_{PS} = 0.5$, $N = 1000$, $\sigma = 0.02$, at different polymer - colloid interaction parameters $\chi_{PC} = \{-0.5, -0.75, -1.0, -1.25\}$
(a) - general view of the polymer density distribution. Polymer density is mapped with blue to yellow palette. Black contour lines trace selected polymer density values. Red viewport highlights space proximal to the embedded particle.
(b) - proximal polymer density change $(\phi - \phi^*)$, where ϕ^* - polymer density of an unperturbed brush.)

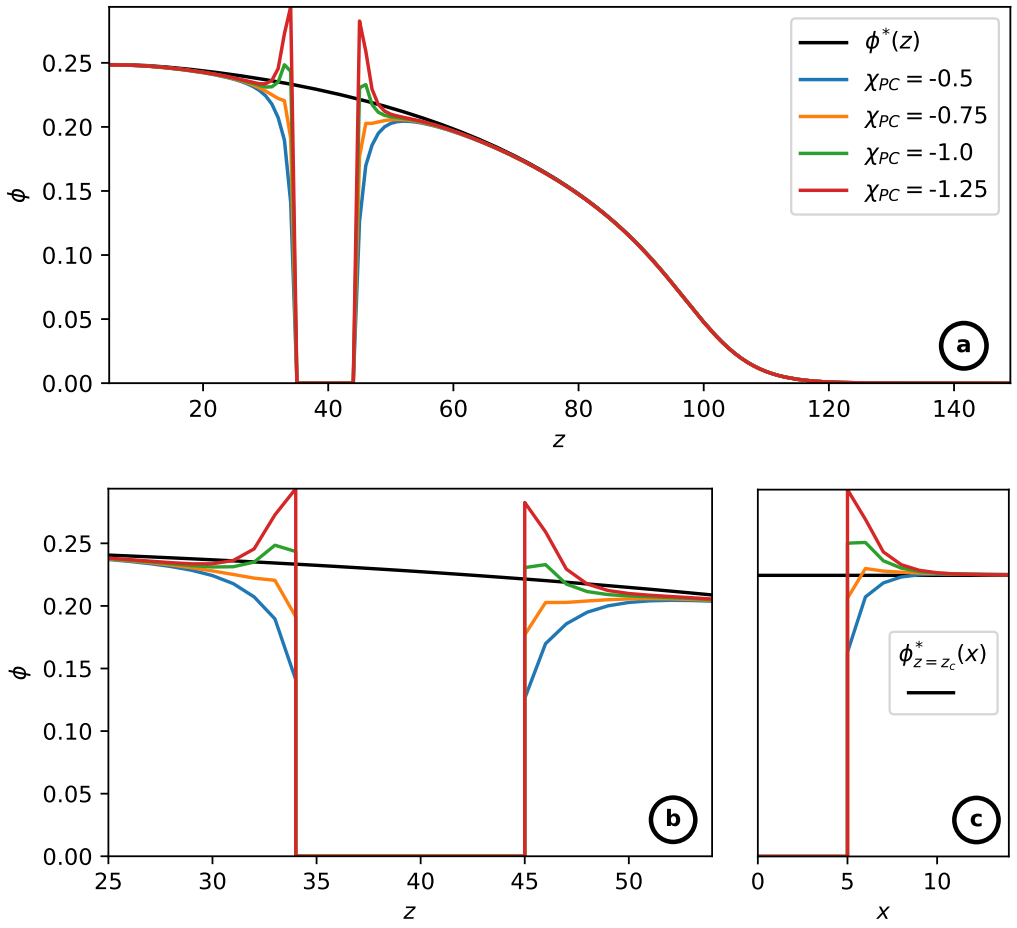

Figure 4: Perturbation of the polymer density profiles in a brush with embedded particle in lineal and lateral directions for $z_c = 40$, $h = w = 10$, $\chi_{PS} = 0.5$, $N = 1000$, $\sigma = 0.02$, at different polymer - particle interaction parameters $\chi_{PC} = \{-0.5, -0.75, -1.0, -1.25\}$ and corresponding polymer volume fraction profile in unperturbed brush (ϕ^*)
(a) - polymer density profile $\phi(z)$ in lineal direction
(b) - polymer density profile $\phi(z)$ in lineal direction, zoomed view
(c) - polymer density profile in lateral direction $\phi(x)_{z=z_c}$

frame in Figures 3a, 3b and blue trace in Figure 4), there is pronounced depletion of the polymer near the embedded particle, which can be seen as the blue halo in Figure 3b. In contrast, around strongly attractive particles $\chi_{PC} = -1.0, -1.25$ (the frames in the second row in Figures 3a,3b and the green and red traces in Figure 4), polymer density is increased in the vicinity of the embedded particle. Note the red halo around the particle in the corresponding frames of Figure 3b.

The behavior of polymer density in the vicinity of the particle in case of $\chi_{PC} = -0.75$ is more complex (see the diagram with the red borders rectangle in Figure 3a and the diagram with red axis spines Figure 3b or the orange color trace in Figure 4). Since $\chi_{PS} = 0.5$ is chosen for these calculations, the value of $\chi_{PC} = -0.75$ at $z_c = 40$ corresponds approximately to critical adsorption conditions, i.e., $\chi_{ads} \approx \chi_{crit}$, so that $\gamma(z_c) \approx 0$. Despite of the vanishing surface term in free energy change $\Delta F_{surf} \sim \gamma \approx 0$, the weak depletion and enrichment regions near the particle are observed.

4.2 Insertion free energy profiles: good solvent conditions, varied polymer-particle interactions

In Figure 5 we present particle insertion free energy profiles $\Delta F(z_c)$ normalized by the particle volume $V = \pi h w^2/4$, for particles with variable dimensions $w = h = \{4, 6, 8, 10, 12\}$, and different strengths of polymer-particle interaction, $\chi_{PC} = \{-0.5, -1.1, -1.5\}$. The solvent is good (athermal) for polymers, $\chi_{PS} = 0$. The case $\chi_{PC} \geq 0$ would corresponds to pure repulsive polymer-particle interactions, whereas at $\chi_{PC} \leq 0$ a short-range attraction operates between monomer units of the brush-forming chains and particle surface.

As a reference line, the osmotic pressure $\Pi(z_c)$ in the particle-free brush is also plotted in Figure 5. It is expected that for large particles or/and vanishing interfacial tension at the particle-polymer solution interface, $\gamma \approx 0$, the normalized insertion free energy profiles $\Delta F(z_c)/V$ should match $\Pi(z_c)$ curves (see eq 8).

As we can see from Figure 5 in the case of weakly attractive, $\chi_{PC} = -0.75$ (or, similarly, repulsive) particle, with $\chi_{ads} \geq \chi_{ads}^{(crit)}$, the normalized insertion free energy $\Delta F(z_c)/V$ curves go systematically beyond $\Pi(z_c)$ because of excess positive free energy contribution due to depletion layer formed by the polymer around the particle, leading to $\gamma \geq 0$. Hence, even without polymer adsorption on the particle, the proportionality of the insertion free energy to the particle volume is violated for sufficiently small particles.

In the case of strongly attractive particle, $\chi_{PC} = -1.5$, $(\chi_{ads} < \chi_{ads}^{(crit)})$

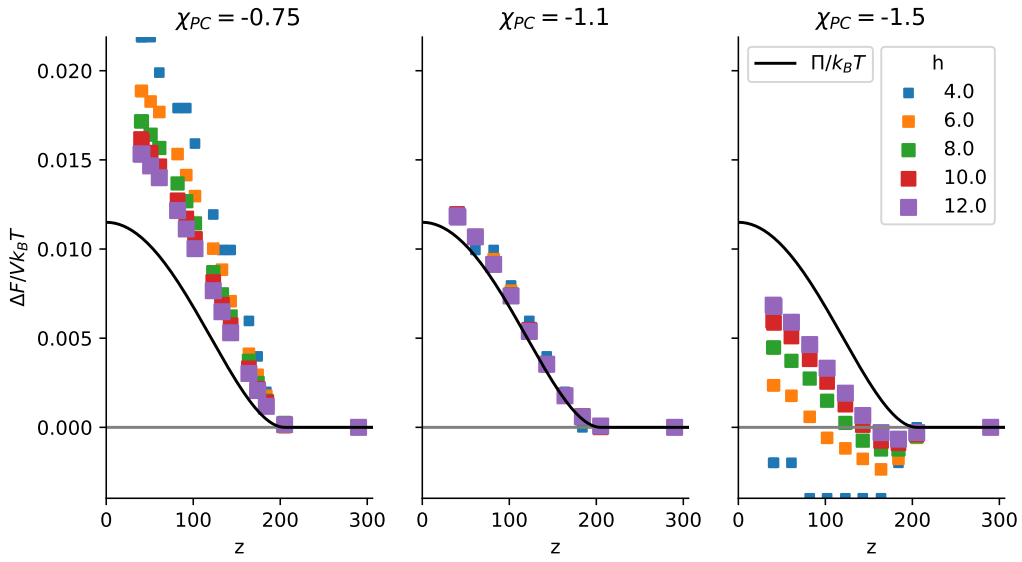

Figure 5: Insertion free energy change $\Delta F(z_c)$ normalized by the particle volume V at different particle center positions z_c, particle sizes $h = w = \{4, 6, 8, 10, 12\}$, particle affinity $\chi_{PC} = \{-0.75, -1.1, -1.5\}$ compared to osmotic pressure profile $\Pi(z)$ for $N = 1000$, $\sigma = 0.02$ in an athermal solvent $\chi_{PS} = 0$

the $\Delta F(z_c)/V$ curves go beneath $\Pi(z_c)$, since $\gamma \leq 0$ and the surface contribution to the insertion free energy is negative. Remarkably, for small particles regions with negative total insertion free energy appears, as the surface contribution outbalances the volume contribution. Which is corresponds to spontaneous particle absorption into such regions of the brush and increased concentration of particles compared to the bulk of the solution, as the partition coefficient becomes $K(z_c) \geq 1$.

As expected, the larger the particle, the smaller its surface-to-volume, A/V ratio, the closer the $\Delta F(z_c)/V$ curves to the osmotic pressure profile $\Pi(z_c)$ are.

The middle drawing of Figure 5 corresponds to the case when $\chi_{ads} \approx \chi_{PC} \approx \chi_{ads}^{(crit)}$ (we remind that here $\chi_{PS} = 0$) and the surface contribution to free energy fairly vanishes, i.e. $\gamma \approx 0$. In this case the normalized free energy $\Delta F(z_c)/V$ curves are close to osmotic pressure profile regardless of the particle size. Indeed, as follows from eq 12 at $\chi_{PS} = 0$, $\chi_{ads} - \chi_{ads}^{(crit)}$ is independent of polymer concentration and can be tuned to zero throughout the brush. For any other arbitrary selected value of $\chi_{PS} \neq 0$ there is no single value of χ_{PC} which would assure that $\chi_{ads} - \chi_{ads}^{(crit)} = 0$ and $\gamma(z_c) = 0$ $\forall z_c \in [0, D]$ and $\Delta F(z_c)/V$ and $\Pi(z_c)$ profiles match each other in the whole z_c range.

4.3 $\gamma(\phi(z))$: Impact of polymer-particle interface

Obviously, $\gamma = \gamma(z)$ essentially depends not only on the set of χ-parameters, but also on local polymer concentration $\phi(z)$. The value of $\gamma\{\chi_{PS}, \chi_{PC}; \phi(z)\}$ can be evaluated from numerical SF-SCF data by subtracting the volume contribution from the calculated insertion free energy, using eq. 11

$$\gamma_{num}(z_c) = \frac{\Delta F(z_c) - \Delta F_{osm}(z_c)}{A} = \frac{\Delta F(z_c)}{A} - \frac{\pi}{A} \int_{z_c - h/2}^{z_c + h/2} \Pi(z') r_c^2(z') dz' \quad (13)$$

where $A = \frac{\pi}{2}(w^2 + 2wh)$ is the particle surface area.

We remind that calculated according to eq 13 value of $\gamma\{\chi_{PS}, \chi_{PC}; \phi(z)\}$ should be considered as an apparent one because the width of the interface between the particle and surrounding polymer solution (the brush interior) in our calculations is comparable to the particle dimensions.

In Figure 6 we present γ as a function of χ_{PC} calculated for selected values of χ_{PS} and different particle position z_c inside the brush using SF-SCF numerical data and eq. 13. The observed trends are consistent with expected dependence $\gamma \sim (\chi_{ads} - \chi_{ads}^{(crit)}) \equiv \chi_{PC} - \chi_{PS}(1 - \phi(z_c)) - \chi_{ads}^{(crit)}$: All

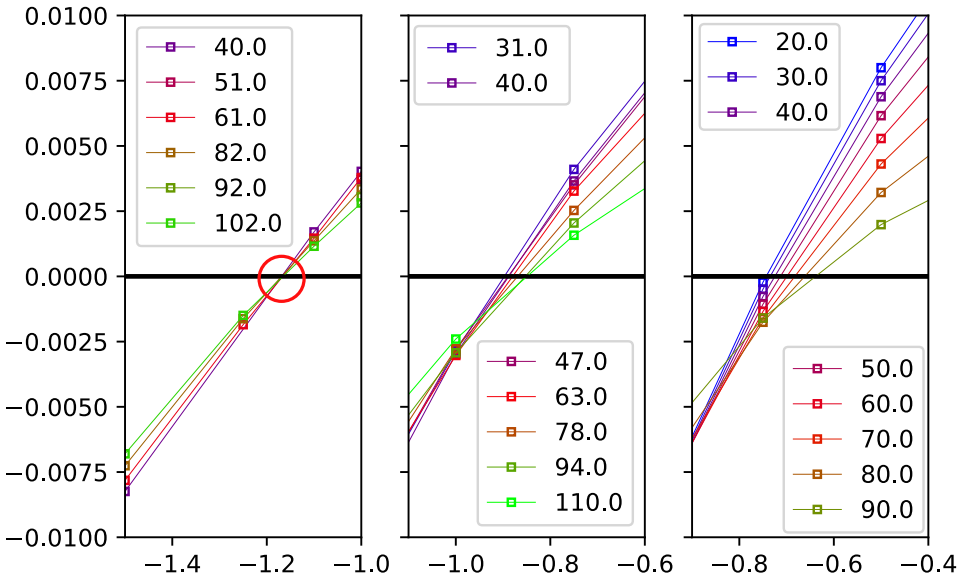

Figure 6: Excess of surface free energy per unit particle area $\gamma(z_c)$ as a function of χ_{PC} at different particle center positions z_c, at different solvent regimes $\chi_{PS} = \{0.0, 0.3, 0.5\}$ for particle size $h = w = 10$, $N = 1000$, $\sigma = 0.02$.
Positions z_c are shown in the legend. Red circe highlights common intersection point.

the curves are approximately linear and cross the horizontal axis (crossover from adsorption to depletion regimes) at $\chi_{PC} = \chi_{PS}(1-\phi(z_c))+\chi_{ads}^{(crit)}$. In the case of athermal solvent, $\chi_{PS} = 0$, all the curves corresponding to different values of z_c (and thus to different local polymer concentrations) cross the horizontal axis in the same point $\chi_{PC} \approx \chi_{ads}^{(crit)}$ (marked with the red circle in Figure 6). For $\chi_{PS} \geq 0$ the value of χ_{PC} corresponding to inversion of sign of γ gets systematically smaller as z_c decreases (i.e. $\phi(z_c)$ increases). This observation illustrates the fact that even if critical adsorption conditions are met at some distance z_c from the surface, they are violated for other particle locations in the brush. Notably, the slope of $\gamma(\chi_{PC}, z_c)$ curves in Figure 6 slightly increases upon a decrease in z_c, that is, upon an increase of local polymer concentration $\phi(z_c)$ inside the brush.

In Figure 7 we present apparent (calculated by eq 13 from numerically evaluated insertion free energy) values of γ at different solvent strength (cor-

responding to different color of the points), different values of the parameter χ_{PC} of polymer-particle interactions and different particle position z_c in the brush. In the 3D plot γ is plotted as a function of $\chi_{ads} = \chi_{PC} - \chi_{PS}(1-\phi(z_c)$ and local polymer concentration $\phi(z_c)$.

Columns of points with the same $\{\chi_{ads}, \phi\}$ correspond to different particle size. Closer inspection indicates that the points get closer to each other upon an increase in the particle size, that is, weakening of the effect of the particle curvature and approaching of the apparent values of γ calculated from eq. 13 to real interfacial tension between polymer solution with concentration ϕ and solid particle.

The set of obtained data points was fitted by the analytical function

$$\gamma(\chi_{ads}, \phi) = (\chi_{ads} - \chi_{ads}^{(crit)})(a_1\phi + a_2\phi^2) \tag{14}$$

where $\chi_{ads} = \phi_{PC} - \phi_{PS}(1-\phi)$ and a_1, a_2 are numerical fitting parameters and we neglected higher order terms in ϕ in the last bracket in eq 14. The rough estimate of a_1 and a_2 are 0.16 and 0.08, respectively.

As follows from eq. 12 and one can see in Figure 7, at sufficiently low polymer concentration in the brush, $\phi \ll 1$, the value of γ is controlled by the parameter $\chi_{ads}(\phi = 0) = \chi_{PC} - \chi_{PS}$. Hence, a decrease in χ_{PC} or/and an increase in χ_{PS} result in stronger polymer affinity to the particle surface and smaller net free energy penalty for the particle insertion into the brush. In the first approximation, the sign of γ is controlled by the difference $\chi_{ads} - \chi_{ads}^{(crit)} \approx \chi_{ads}(\phi = 0) - \chi_{ads}^{(crit)} \approx \chi_{PC} - \chi_{PS} - \chi_{ads}^{(crit)}$.

Note that, $\frac{d\gamma}{d\chi_{ads}} = (a_1\phi + a_2\phi^2)$ so the slope of $\gamma(\chi_{ads})$ increases with polymer concentration, which can be seen as a counter-clockwise rotation of the grey surface around the $\chi_{ads} = \chi_{ads}^{(crit)}$ line. Thus the sign of γ remains the same for $\chi_{ads}(\phi = 0)$ and χ_{ads} at arbitrary ϕ or z. Since χ_{ads} is a function of ϕ too - the aforesaid approximation is invalid for arbitrary ϕ especially in the poor solvent regime with $\chi_{PS} > 0.5$. With higher values of χ_{PS} and ϕ the approximation gets off, underestimating γ.

The region with $\phi(z) \ll 1$ in poor solvent regime is either absent or has a very narrow interval of z, $\phi(z)$ profile according to ASCF predictions is not continuous and has a sharp edge, numerical results confirms this prediction exhibiting very steep change in polymer concentration at the polymer brush's edge. In Figure 7 this caused the absence of numerical results for $\chi_{PS} = 0.6$ in low concentration range.

Having $\gamma(\chi_{ads}, \phi)$ calculated, we can evaluate insertion free energy as

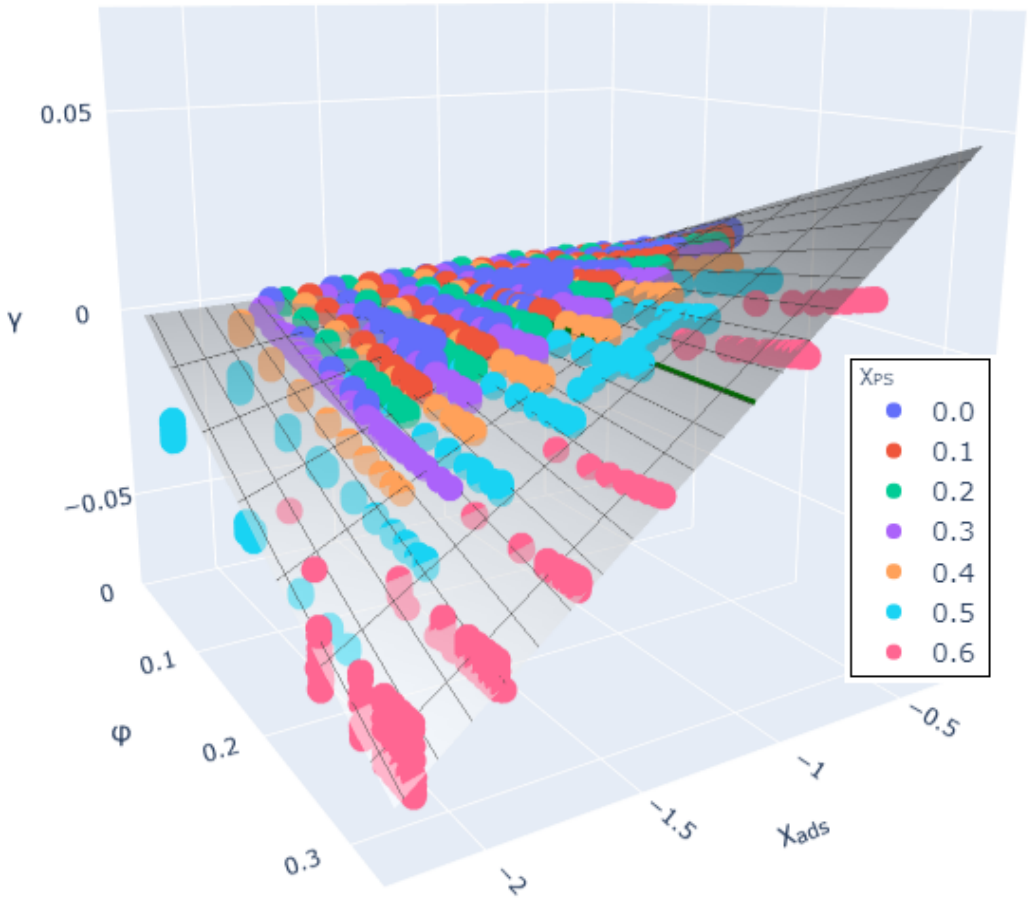

Figure 7: The dependence of γ and γ_{num} on $\{\chi_{ads}, \phi(z)\}$ at different solvent regimes $\chi_{PS} \in [0.0, 0.6]$ and particle affinity to the polymer $\chi_{PC} \in [-1.5, -0.5]$ for $N = 1000$, $\sigma = 0.02$
SF-SCF numerical results (scatter) and corresponding analytical model surface. Green line corresponds to $\gamma = 0$

$$\Delta F(\chi_{PS}, \chi_{PC}, \phi\{z_c\}) =$$
$$\pi\frac{w^2}{4}\int_{z_c-h/2}^{z_c+h/2}\Pi(\phi(z'))dz' + \frac{\pi}{2}(2wh+w^2)\gamma(\chi_{PS}, \chi_{PC}, \phi\{z_c\}) \quad (15)$$

where the osmotic pressure $\Pi(\phi(z))$ is given by eq 5 and we use the polymer density profile $\phi(z)$ calculated by SF-SCF method for the particle-free (unperturbed) brush.

In Figure 8 we compare theoretically calculated (by eq 15) insertion free energy (red trace) with SC-SCF numeric results (blue scatter). The analytically calculated osmotic term $\Delta F_{osm}(z_c)$ and interfacial term $\Delta F_{surf}(z_c)$ are presented by grey dashed line and grey dotted line, respectively. The results are presented for selected values of $\chi_{PS} = \{0.0, 0.3, 0.6\}$ and $\chi_{PC} = \{-0.5, -1.0, -1.5\}$ for a cylindrical particle with dimensions $h = w = 10$.

The solvent quality is decreasing from the left (athermal solvent, $\chi_{PS} = 0$) to the right (down to moderately poor solvent, $\chi_{PS} = 0.6$).

According to ASCF, for the poor solvent regime $\chi_{PS} > 0.5$ the polymer concentration profile became a step-like function, with $\phi(z = 0) \neq 0$. Using ASCF approximation, polymer concentration for a brush with $N = 1000$ and $\sigma = 0.02$ at $\chi_{PS} = 0.6$ has been evaluated to be $\phi(z = 0) \approx 0.325$, $\phi(z = D) \approx 0.245$ where $D \approx 66.2$, which can also be seen in the Figure 2. In Figure 8 the right panel correspond to the poor solvent regime, thus covers only the cases where $\phi \notin [0, \phi(z = 0)]$. Note that $\chi_{ads} \approx \chi_{ads}(\phi = 0)$ can not deliver right result and more rigorous eq. 12 has to be used.

The polymer-particle contact attraction energy is increasing from up to down. The adsorption strength $|\chi_{ads}| = |\chi_{PC} - \chi_{PS}(1 - \phi)|$ for a given ϕ is thus increasing from upper left to lower right corner.

In the upper line $\chi_{PC} = -0.5$ and at any solvent quality $\chi_{ads} \geq \chi_{ads}^{(crit)}$, that is, there is a depletion layer around the particle. For $\chi_{PS} = 0.6$ for $\forall\phi \in [\phi(z = D), \phi(z = 0)]$ $\gamma > 0$. As a result, $\gamma \geq 0$ and both, the osmotic and the surface contributions to ΔF_{z_c} are positive though decreasing in magnitude upon a decrease in solvent strength.

The middle line corresponds to moderately strong polymer colloid attraction, $\chi_{PC} = -1.0$. At $\chi_{PS} = 0$ and $\chi_{PS} = 0.3$ nearly critical adsorption conditions, $\chi_{ads} \approx \chi_{ads}^{(crit)}$ are fulfilled and surface contribution $\Delta F_{surf} \sim \gamma$ to the free energy fairly vanishes. The net free energy is dominated by the osmotic term. Under poor solvent conditions , $\chi_{PS} = 0.6$ adsorption of polymer on the particle takes place, because $\chi_{ads} = \chi_{PC} - \chi_{PS}(1 - \phi) \leq \chi_{ads}^{(crit)}$, $\forall\phi \in [\phi(z = D), \phi(z = 0)]$, $\gamma < 0$ and, as a result, negative surface free energy overcompensate weak positive osmotic contribution: the free energy balance upon particle embedding into the brush is negative.

The lower line in Figure 8 corresponds to strong polymer-particle attraction, $\chi_{PC} = -1.5$, that is, polymer is adsorbed onto the particle surface, $\chi_{ads} \leq \chi_{ads}^{(crit)}$ irrespectively of the solvent strength. Under good solvent conditions, χ_{PS}, the left panel, the insertion free energy is dominated by osmotic repulsion and is positive at any particle position, except the very edge of the brush, where polymer concentration is low and osmotic repulsion is insufficient to overcome gain the free energy due to adsorption of terminal segments of the brush forming chains onto the particle: As a result, a shallow potential well emerge at the periphery of the brush. Upon a decrease in the solvent strength (an increase in χ_{PS}) the adsorption strength increases whereas the magnitude of osmotic repulsion decreases. As a result, the minimum in the insertion free energy becomes more pronounced and extends deeper into the brush. Only in the pre-surface region with higher polymer concentration the osmotic repulsion dominates over attractive surface term. Eventually, under poor solvent conditions (lower right corner of the Figure), osmotic contribution is small whereas adsorption strength is large so that $\Delta F(z_c)$ is negative throughout the brush, which implies spontaneous accumulation of particles in the brush due to high polymer-particle affinity; the osmotic repulsive term $\Delta F_{osm} \geq 0$ under these conditions is negligible $\forall z \in [0, D]$.

Altogether, Figure 8 demonstrates good quantitative agreement between insertion free energy profiles $\Delta F(z_c)$ obtained by exact numerical SF-SCF calculations and by approximate analytical approach.

4.4 Effects of particle size and shape

As discussed above, in the cases of inert or weakly attractive for polymer segments particle, both terms in the insertion free energy are positive and $\Delta F(z_c)$ monotonously grows upon a decrease in z_c (deeper embedding of the particle into the brush). If $\chi_{ads} \leq \chi_{ads}^{(crit)}$ and $\gamma \leq 0$, then the short-range attraction operating between polymer segments and the particle leads to (partial) cancellation of the osmotic penalty for the particle insertion into the brush. However, for large particle the osmotic contribution, which is proportional to the particle volume, remains dominant even if the brush-forming chains do adsorb onto the particle surface, $\gamma \leq 0$.

In Figure 9 we plot $\Delta F/V$ as a function of χ_{ads} at constant z_c for varied particle volume V (the case of $d = h$) and varied solvent strength.

The osmotic pressure $\Pi(\phi(z_c)$ at given distance $z = z_c$ is controlled by grafting density σ, degree of polymerization N and the solvent strength χ_{PS}. Hence, for a given particle position the osmotic pressure is a function of χ_{PS}, which is depicted by horizontal lines on Figure 9.

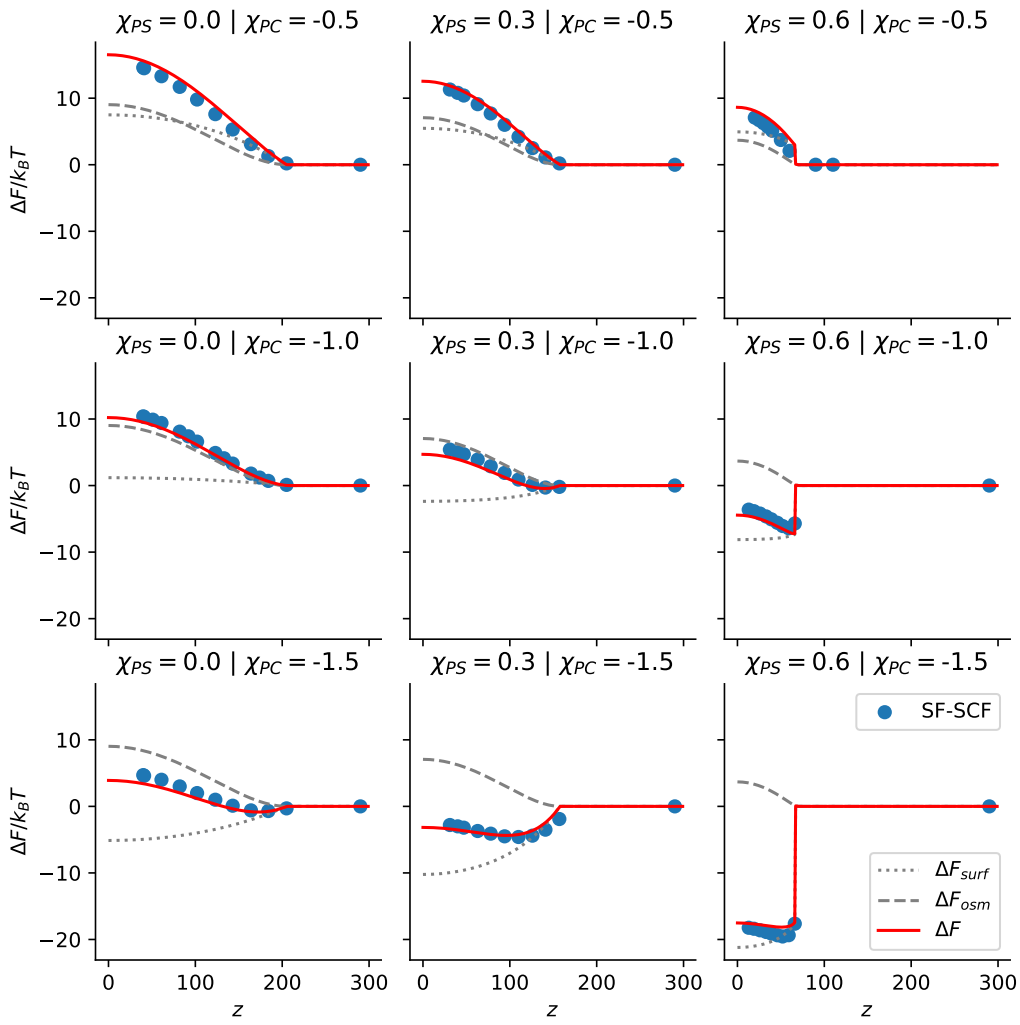

Figure 8: Apparent insertion free energy ΔF on z_c at $\chi_{PS} = \{0.0, 0.3, 0.6\}$ and $\chi_{PC} = \{-0.5, -1.0, -1.5\}$ for $N = 1000$, $\sigma = 0.02$, $h = w = 10$. SF-SCF numerical results (scatter) and analytical model (red line). By gray dashed and dotted lines the osmotic, $\Delta F_{osm}(z_c)$ and the surface, $\Delta F_{surf}(z_c)$, contributions to the analytically calculated free energy are depicted.

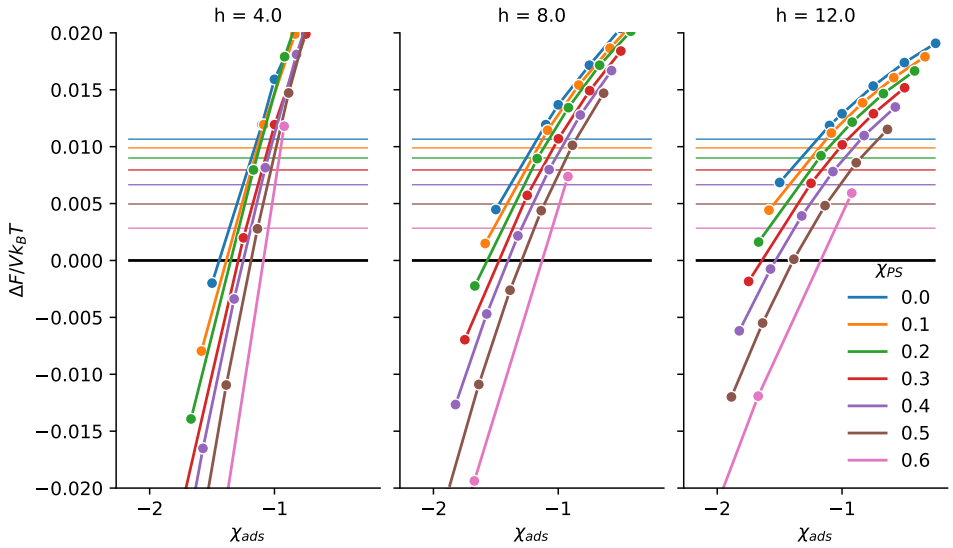

Figure 9: The dependence of $\Delta F/V$ on χ_{ads} and Π/k_BT at different particle volumes $h = w = \{4, 8, 12\}$ and solvent regimes $\chi_{PS} = \{0, 0.1, 0.2, 0.3, 0.4, 0.5, 0.6\}$ for $N = 1000$, $\sigma = 0.02$ and $z_c = 40$
(scatter) - SF-SCF numerical results
(horizontal lines) - $\Pi(z_c, \chi_{PS})/k_BT$

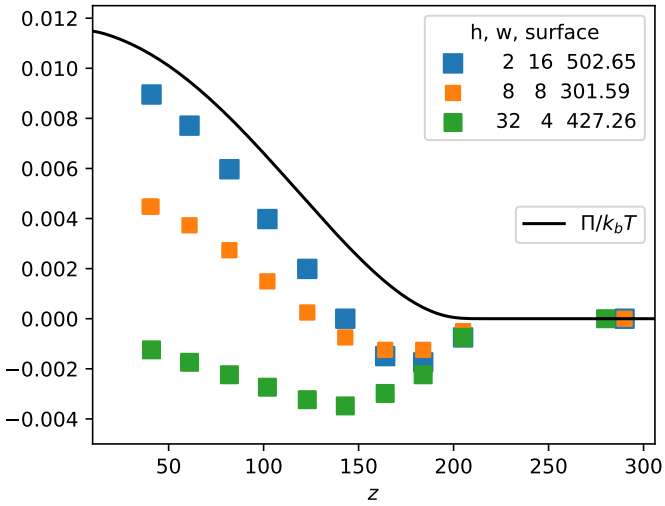

Figure 10: The dependence of $\Delta F/V$ on particle geometry $(h, w) = \{(2, 16), (8, 8), (32, 4)\}$ with fixed particle volume for $\chi_{PS} = 0$, $\chi_{PC} = -1.5$, $N = 1000$ and $\sigma = 0.02$ compared to the osmotic pressure profile $\Pi(z)/k_BT$ of corresponding unperturbed brush

The normalized by the particle volume insertion free energy then can be approximated as

$$\frac{\Delta F(z_c, \chi_{PS}, \chi_{PC})}{V} \approx \Pi(z_c, \chi_{PS}) + \gamma(z_c, \chi_{PS}, \chi_{PC})\frac{A}{V} \tag{16}$$

in the limit of large particles $\frac{A}{V} \to 0$, thus

$$\frac{\Delta F(z_c, \chi_{PS})}{V} \approx \Pi(z_c, \chi_{PS}) \tag{17}$$

As the particles get bigger the contribution related to the particle surface have less impact on the overall apparent insertion free energy. In Figure 9 we see that the slope of SF-SCF numerical results decreases with an increasing particle volume. For sufficiently big particles the curves are expected to collapse to horizontal lines $\Pi(z_c, \chi_{PS})$.

The $\Delta F(z_c)$ curves may acquire more complex shape for adsorbing polymer particles, $\gamma \leq 0$, with smaller volume-to-surface ratio, that is for sufficiently small and asymmetric ($h \ll d$ or $d \ll h$) particles.

In Figure 10 we present $\Delta F(z_c)$ curves for adsorbing polymer particles with constant volume and varied ratio d/h for $\gamma \leq 0$.

Intuitively it is expected that an increase in A/V ratio would cause surface term in free energy ΔF_{surf} to grow in magnitude proportional to the particle surface A, while osmotic term proportional to the particle volume remains constant. So the curves should go systematically beneath the osmotic pressure profile in a manner, that the higher value of A is, the lower the corresponding curve goes, since $\gamma \leq 0$. Thus we should have observed the next order in which all the curves lie in Figure 10: the particle with $h = 8, w = 8$ would be the closest to $\Pi(z)/k_BT$ profile, having the smallest surface; the particle with $h = 2, w = 16$, on the other hand, would be the lowest one.

As we can see Figure 10 SF-SCF numerical results evidence more complex behavior of the ΔF_{z_c} as a function of the particle shape. As expected, the insertion free energy for "cigar-like" particle ($h = 32, w = 4$) is systematically lower than for a symmetric ($h = 8, w = 8$) particle with the same volume because of larger surface area A for the former one: the minimum in $\Delta F(z_c)$ is shifted towards center of the brush and gets deeper. However, the profile of the insertion free energy $\Delta F(z_c)$ for the disk-like particle ($h = 2, w = 16$) is going beyond that for the symmetric particle, particularly in the inner denser part of the brush in spite of larger surface area of the disk. This effect can be attributed to stronger perturbation of conformations of the brush-forming chains upon embedding of the disk-like particle in quanched orientation with the base parallel to the grafting surface. A proper account of rotational

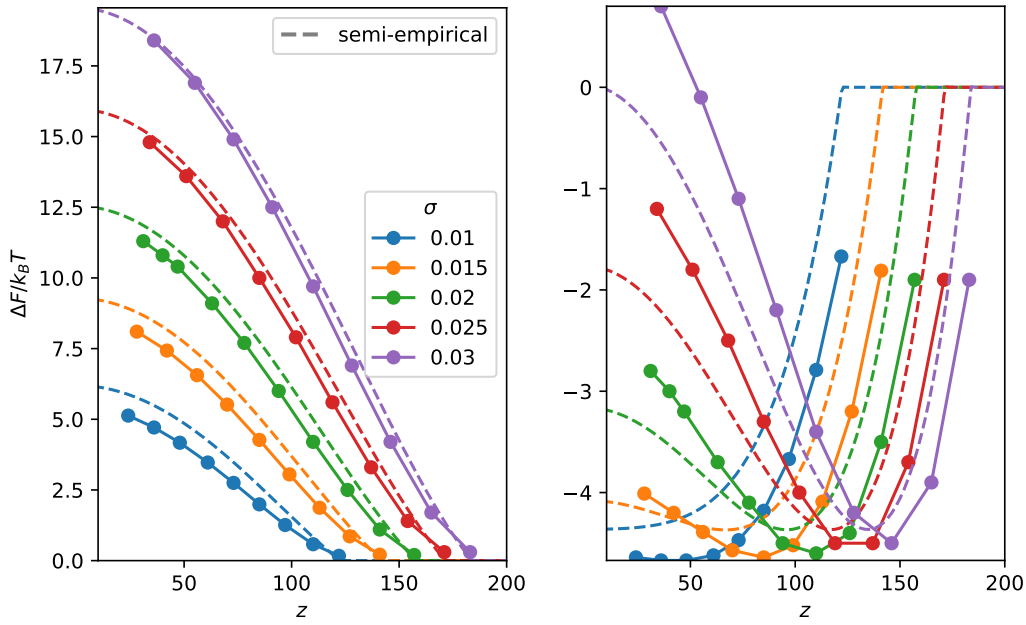

Figure 11: Apparent insertion free energy change ΔF on z_c at $\sigma = \{0.01, 0.015, 0.02, 0.025, 0.03\}$ and $\chi_{PC} = \{-0.5, -1.5\}$ for $w = h = 10$, $\chi_{PS} = 0.3$ and $N = 1000$. SF-SCF numerical results (connected dots) and analytical model (dashed lines). Weak adsorbing particles ($\chi_{PC} = -0.5$) on the left and strong adsorbing particles ($\chi_{PC} = -1.5$) on the right

diffusion may lead to systematically lower free energy of the disc-like particle penetrating into the brush.

4.5 Effects of grafting density

Evidently, an increase in grafting density leads to both an increase in the brush thickness and (under good and theta-solvent conditions) to an increase in the polymer concentration in the brush. As soon as polymer density $\phi(z_c)$ affects in a different ways the osmotic and to the surface parts of the insertion free energy, we may expect that increasing grafting density may affect not only the extension and the magnitude, but also the shape of the insertion free energy $\Delta F(z_c)$ profiles.

The result of SF-SCF numerical calculations for varied grafting density σ compared to the predictions of the analytical model presented in Figure 11.

As expected, for non-adsorbing polymer particles, the magnitude of $\Delta F(z_c)$ progressively increases and the onset of the brush-particle repulsion is shifted to larger z_c (due to increasing brush thickness) upon an increase in grafting

density.

On the contrary, in the case of polymer-adsorbing ($\chi_{ads} \leq \chi_{ads}^{(crit)}$ particles, at large grafting densities pronounced peripheral minimum and proximal to the grafting surface maximum are observed. A decrease in the grafting density leads to a significant decrease in the maximum magnitude (and its eventual disappearance) and simultaneous deepening and widening of the the peripheral minimum in the insertion free energy profiles.

5 Discussion and conclusions

We have used self-consistent field SF-SCF numerical method to study insertion of a (nano)colloidal particle into a polymer brush. The effect of embedded particle on the polymer density distribution in the brush and the free energy penalty (or gain) upon particle insertion into the brush were analyzed. The latter controls equilibrium partitioning of particles between the brush and surrounding solution.

The position-dependent insertion free energy of the particle in the brush was analyzed as a function of (i) thermodynamic quality of the solvent for the polymer; (ii) short-range polymer-particle attraction/repulsion; (iii) particle size and shape; (iv) grafting density of polymer chains. The effect of embedded particle on the density distribution of polymer in the brush was analyzed as well.

The obtained by numerical SF-SCF method insertion free energy profiles were systematically compared to those calculated within approximate analytical scheme. The latter was developed using strong stretching self-consistent field theory of polymer brushes and is based on the assumption that the insertion free energy can be decoupled into two contributions proportional to the partial volume and partial surface, respectively. This decoupling scheme is asymptotically exact for large particles embedded in quasi-infinite reservoir of polymer solution. However, it can serve as a quantitatively reasonable approximation even for small particles inserted into finite-size brush considered here.

The free energy term ΔF_{osm} proportional to the product of particle volume and local osmotic pressure is always positive and provides repulsive contribution to the net free energy balance. It grows upon increasing solvent strength and grafting density. For sufficiently large particles this term is always the dominant one. However, for the particles of small size and thus smaller surface-to-volume ratio the surface-related contribution ΔF_{surf} may be comparable and even outperforming the volume term. As a result, in the case of short-range attractive interactions between polymer chains and

the particle surface the net insertion free energy may become negative. We remind that for small particles splitting of the free energy into volume and surface controlled terms is ambiguous and can serve only as an approximation.

Depending on the sign of ΔF and shape of insertion free energy profile, different scenario of particle exclusion from or accumulation in the brush may take place.

If the particles are "inert" or weakly adsorbing for polymer chains, the insertion free energy profile has a shape of a potential barrier with the height increasing towards grafting surface. Remarkably, both the width (extension) and the magnitude of the barrier can be efficiently controlled by solvent strength for the brush-forming chains and decrease upon a decrease in the solvent strength. At given solvent strength the insertion free energy grows upon an increase in the grafting density, but is relatively insensitive to the DP of the brush-forming chains (the latter parameter affects primarily the width of the barrier). Hence, an increase in either grafting density or/and in solvent strength lead to exclusion of particles from the brush. This is a target in application of water-soluble polymer brushes in prevention of non-specific protein adsorption and design of antifouling surfaces.

The short-range attractive interactions between the particle and polymer chains may not only reduce the free energy penalty for particle insertion into the brush and lower the potential barrier, but also qualitatively change the insertion potential profile. The latter may acquire non-monotonic shape and exhibit local minima at the periphery of the brush followed by a repulsive barrier close to the grafting surface. The height of this barrier decreases upon increasing polymer-particle attraction energy or/and decreasing grafting density. In this case instead of exclusion, the particles will be accumulated inside the brush. Hence, our theory explains maximum in the dependence of absorbed by the brush number of nanoparticles on the brush grafting density, as observed in experiments.[40,41]

As demonstrated above, the shape of the $\Delta F(z)$ curves can be tuned not only by solvent strength or polymer-particle affinity, but also by changing surface-to-volume ratio which depends on the size and shape asymmetry of the particles. This allows, for example, separating particles with respect to their shape.

We remind that within our theory we disregard either direct or indirect (by perturbation of the structure of the brush) interactions between the particles localized inside the brush. Hence, this theory is applicable at sufficiently low particle concentration inside the brush which is usually the case for pure repulsive shape of ΔF, though may be violated upon accumulation of particles in the brush.

If the brush is tethered to a (semi) permeable membrane, tuning of the width and shape of the barrier by changing solvent strength may allow controlling permeability of the polymer-modified membrane for particles. Obtained in this work results allow us to study quantitatively diffusion of particles across membrane-attached polymer brushes that will be in the scope of the forthcoming publication. Furthermore, because the developed in the present paper scheme enables calculating the insertion free energy as a function of local polymer concentration, solvent strength and polymer-particle interaction parameter, it can be further applied to analysis of partitioning and diffusion of nanoparticles in polymer brushes of more complex architectures, e.g., in polymer-modified nanopores.

Acknowledgments

This work was supported by Russian Foundation for Basic Research, grant 21-53-10005.

References

(1) Klein, J. Polymers in living systems: From biological lubrication to tissue engineering and biomedical devices. *Polymers for Advanced Technologies* **2012**, *23*, 729–735.

(2) Camesano, T. A.; Abu-Lail, N. I. Heterogeneity in bacterial surface polysaccharides, probed on a single-molecule basis. *Biomacromolecules* **2002**, *3*, 661–667.

(3) Vu, B.; Chen, M.; Crawford, R. J.; Ivanova, E. P. Bacterial extracellular polysaccharides involved in biofilm formation. *Molecules* **2009**, *14*, 2535–2554.

(4) Avila-Calderón, E. D.; Ruiz-Palma, M. d. S.; Aguilera-Arreola, M. G.; Velázquez-Guadarrama, N.; Ruiz, E. A.; Gomez-Lunar, Z.; Witonsky, S.; Contreras-Rodríguez, A. Outer Membrane Vesicles of Gram-Negative Bacteria: An Outlook on Biogenesis. *Frontiers in Microbiology* **2021**, *12*, 345.

(5) Suntharalingam, M.; Wente, S. R. Peering through the pore: Nuclear pore complex structure, assembly, and function. **2003**, *4*, 775–789.

(6) Kubitscheck, U.; Grünwald, D.; Hoekstra, A.; Rohleder, D.; Kues, T.; Siebrasse, J. P.; Peters, R. Nuclear transport of single molecules: Dwell times at the nuclear pore complex. *Journal of Cell Biology* **2005**, *168*, 233–243.

(7) Tu, L. C.; Fu, G.; Zilman, A.; Musser, S. M. Large cargo transport by nuclear pores: Implications for the spatial organization of FG-nucleoporins. *EMBO Journal* **2013**, *32*, 3220–3230.

(8) Fu, G.; Tu, L. C.; Zilman, A.; Musser, S. M. Investigating molecular crowding within nuclear pores using polarization-PALM. *eLife* **2017**, *6*, DOI: 10.7554/eLife.28716.

(9) Denning, D. P.; Patel, S. S.; Uversky, V.; Fink, A. L.; Rexach, M. Disorder in the nuclear pore complex: The FG repeat regions of nucleoporins are natively unfolded. *Proceedings of the National Academy of Sciences of the United States of America* **2003**, *100*, 2450–2455.

(10) Yang, W.; Musser, S. M. Nuclear import time and transport efficiency depend on importin β concentration. *Journal of Cell Biology* **2006**, *174*, 951–961.

(11) *Biosensors*; Cooper, J., Cass, A., Eds.; Practical approach series; Oxford University Press: 2004.

(12) Chen, W. L.; Cordero, R.; Tran, H.; Ober, C. K. 50th Anniversary Perspective: Polymer Brushes: Novel Surfaces for Future Materials. *Macromolecules* **2017**, *50*, 4089–4113.

(13) Halperin, A. Polymer brushes that resist adsorption of model proteins: Design parameters. *Langmuir* **1999**, *15*, 2525–2533.

(14) Ayres, N. Polymer brushes: Applications in biomaterials and nanotechnology. *Polymer Chemistry* **2010**, *1*, 769–777.

(15) Krishnamoorthy, M.; Hakobyan, S.; Ramstedt, M.; Gautrot, J. E. Surface-initiated polymer brushes in the biomedical field: Applications in membrane science, biosensing, cell culture, regenerative medicine and antibacterial coatings. *Chemical Reviews* **2014**, *114*, 10976–11026.

(16) Doberenz, F.; Zeng, K.; Willems, C.; Zhang, K.; Groth, T. Thermoresponsive polymers and their biomedical application in tissue engineering-A review. *Journal of Materials Chemistry B* **2020**, *8*, 607–628.

(17) *Responsive Polymer Materials: Design and Applications*; Minko, S., Ed.; Wiley: 2006, p 288.

(18) Nishiyama, N.; Kataoka, K. Nanostructured devices based on block copolymer assemblies for drug delivery: Designing structures for enhanced drug function. **2006**, *193*, 67–101.

(19) Schacher, F. H.; Rupar, P. A.; Manners, I. Functional block copolymers: Nanostructured materials with emerging applications. **2012**, *51*, 7898–7921.

(20) Sakai-Kato, K.; Nishiyama, N.; Kozaki, M.; Nakanishi, T.; Matsuda, Y.; Hirano, M.; Hanada, H.; Hisada, S.; Onodera, H.; Harashima, H.; Matsumura, Y.; Kataoka, K.; Goda, Y.; Okuda, H.; Kawanishi, T. General considerations regarding the in vitro and in vivo properties of block copolymer micelle products and their evaluation. **2015**, *210*, 76–83.

(21) Betageri, G. V.; Enkins, S. a.; Parsons, D. L., *Liposome Drug Delivery Systems*; CRC Press: London, 1993, p 148.

(22) *Stealth liposomes*; Lasic, D. D., Martin, F. J., Mayhew, E., Eds.; CRC Press: London, 1991, p 320.

(23) Norde, W.; Gags, D. Interaction of bovine serum albumin and human blood plasma with PEO-tethered surfaces: Influence of PEO chain length, grafting density, and temperature. *Langmuir* **2004**, *20*, 4162–4167.

(24) Bosker, W. T.; Iakovlev, P. A.; Norde, W.; Cohen Stuart, M. A. BSA adsorption on bimodal PEO brushes. *Journal of Colloid and Interface Science* **2005**, *286*, 496–503.

(25) Kim, J. U.; O'Shaughnessy, B. Morphology Selection of Nanoparticle Dispersions by Polymer Media. *Phys. Rev. Lett.* **2002**, *89*, 238301.

(26) Halperin, A. Polymer brushes that resist adsorption of model proteins: Design parameters. *Langmuir* **1999**, *15*, 2525–2533.

(27) Halperin, A.; Fragneto, G.; Schollier, A.; Sferrazza, M. Primary versus ternary adsorption of proteins onto PEG brushes. *Langmuir* **2007**, *23*, 10603–10617.

(28) Halperin, A.; Zhulina, E. Atomic force microscopy of polymer brushes: colloidal versus sharp tips. *Langmuir* **2010**, *26*, 8933–8940.

(29) Murat, M.; Grest*, G. S. Molecular Dynamics Simulations of the Force between a Polymer Brush and an AFM Tip. *Macromolecules* **1996**, *29*, 8282–8284.

(30) Ermilov, V.; Lazutin, A.; Halperin, A. Colloids in brushes: The insertion free energy via monte carlo simulation with umbrella sampling. *Macromolecules* **2010**, *43*, 3511–3520.

(31) Halperin, A.; Kröger, M.; Zhulina, E. B. Colloid-brush interactions: The effect of solvent quality. *Macromolecules* **2011**, *44*, 3622–3638.

(32) Fleer, G.; Stuart, M.; Scheutjens, J.; Cosgrove, T.; Vincent, B., *Polymers at Interfaces*; Springer Netherlands: 1993.

(33) Zhulina, E. B.; Pryamitsyn, V. A.; Borisov, O. V. Structure and conformational transitions in grafted polymer chain layers. A new theory. *Polymer Science U.S.S.R.* **1989**, *31*, 205–216.

(34) Zhulina, E. B.; Borisov, O. V.; Pryamitsyn, V. A.; Birshtein, T. M. Coil-Globule Type Transitions in Polymers. 1. Collapse of Layers of Grafted Polymer Chains. *Macromolecules* **1991**, *24*, 140–149.

(35) Lebedeva, I. O.; Zhulina, E. B.; Leermakers, F. A.; Borisov, O. V. Dendron and Hyperbranched Polymer Brushes in Good and Poor Solvents. *Langmuir* **2017**, *33*, 1315–1325.

(36) Birshtein, T. M.; Zhulina, E. B.; Skvortsov, A. M. Adsorption of polypeptides on solid surfaces. I. Effect of chain stiffness. *Biopolymers* **1979**, *18*, 1171–1186.

(37) Birshtein, T. M.; Zhulina, E. B. Conformations of polymer chains grafted to an impermeable plane surface. *Polymer Science U.S.S.R.* **1983**, *25*, 2165–2174.

(38) Eisenriegler, E.; Kremer, K.; Binder, K. Adsorption of polymer chains at surfaces: Scaling and Monte Carlo analyses. *The Journal of Chemical Physics* **1982**, *77*, 6296–6320.

(39) Grosberg, A. Y.; Khokhlov, A. R., *Statistical Physics of Macromolecules*; American Institute of Physics: New York, 1994, p 350.

(40) Gage, R. A.; Currie, E. P. K.; Stuart, M. A. C. Adsorption of Nanocolloidal SiO2 Particles on PEO Brushes. *Macromolecules* **2001**, *34*, 5078–5080.

(41) Mora-Sierra, Z.; Gopan, G.; Chang, R.; Leckband, D. E.; Gruebele, M. Stabilization and Kinetics of an Adsorbed Protein Depends on the Poly(N-isopropylacrylamide) Grafting Density. *Biomacromolecules* **2021**, *22*, DOI: 10.1021/acs.biomac.1c00417.